

# Empirical constraints on the high-density equation of state from multi-messenger observables

Márcio Ferreira,<sup>1,\*</sup> M. Fortin,<sup>2</sup> Tuhin Malik,<sup>3</sup> B. K. Agrawal,<sup>4,5</sup> and Constança Providência<sup>1</sup>

<sup>1</sup>*CFisUC, Department of Physics, University of Coimbra, P-3004 - 516 Coimbra, Portugal*

<sup>2</sup>*N. Copernicus Astronomical Center, Polish Academy of Science, Bartycka,18, 00-716 Warszawa, Poland*

<sup>3</sup>*BITS-Pilani, Department of Physics, K.K. Birla Goa Campus, GOA - 403726, India*

<sup>4</sup>*Saha Institute of Nuclear physics, Kolkata 700064, India*

<sup>5</sup>*Homi Bhabha National Institute, Anushakti Nagar, Mumbai - 400094, India*

(Dated: December 25, 2019)

We search for possible correlations between neutron star observables and thermodynamic quantities that characterize high density nuclear matter. We generate a set of model-independent equations of state describing stellar matter from a Taylor expansion around saturation density. Each equation of state which is a functional of the nuclear matter parameters is thermodynamically consistent, causal and compatible with astrophysical observations. We find that the neutron star tidal deformability and radius are strongly correlated with the pressure, the energy density and the sound velocity at different densities. Similar correlations are also exhibited by a large set of mean-field models based on non-relativistic and relativistic nuclear energy density functionals. These model independent correlations can be employed to constrain the equation of state at different densities above saturation from measurements of NS properties with multi-messenger observations. In particular, precise constraints on the radius of PSR J0030+0451 thanks to NICER observations would allow to better infer the properties of matter around two times the nuclear saturation density.

## I. INTRODUCTION

The properties of the equation of state (EoS) of nuclear matter at supra-saturation densities, that is above the nuclear saturation density  $n_0 \sim 0.16 \text{ fm}^{-3}$ , still remain an open question in nuclear physics. Neutron stars (NSs) are unique astrophysical objects through which the properties of super-dense neutron-rich nuclear matter at zero temperature can be studied. Constraining the EoS requires combining astrophysics and nuclear physics. Astrophysical observations are important probes for the dense nuclear matter properties. Several NSs with a mass about two-solar masses detected during the last decade set quite stringent constraints on EoS of nuclear matter. The pulsar PSR J1614–2230 is, among the most massive observed pulsars, the one with the smallest uncertainty on the mass  $M = 1.906 \pm 0.016 M_\odot$  [1–3] (masses are reported with  $1\sigma$  error-bars or equivalently 68.3% credibility intervals throughout this work). Other two pulsars with a mass above two solar masses are PSR J0348+0432 with  $M = 2.01 \pm 0.04 M_\odot$  [4] and the recently detected MSP J0740+6620 with a mass  $2.14^{+0.10}_{-0.09} M_\odot$  [5].

Detecting gravitational waves (GWs) emitted during the coalescence of binary NS systems is also one of the most promising way to probe high density behavior of the EoS for dense stellar matter. The analysis of the compact binary inspiral event GW170817 has placed upper bounds on the NS combined dimensionless tidal deformability [6]. Using a low-spin prior (consistent

with the observed NS population), the combined dimensionless tidal deformability of the two NSs that merged during the event was determined to be  $\tilde{\Lambda} \leq 800$  with 90% confidence. A follow up reanalysis [7] assuming the same EoS for the two NSs and for a spin range consistent with the one observed in Galactic binary NSs obtained  $\tilde{\Lambda} \leq 900$  and the tidal deformability of a 1.4 solar mass NS was estimated to be  $70 < \Lambda_{1.4M_\odot} < 580$  at the 90% level. The detection of GWs from the GW170817 event was followed by the electromagnetic counterpart, the gamma-ray burst (GRB) GRB170817A [8], and the electromagnetic transient AT2017gfo [9], that set extra constraints on the lower limit of the tidal deformability [10–14]. This last constraint seems to rule out very soft EoS: the lower limit of the tidal deformability of a  $1.37M_\odot$  star set by the above studies limits the tidal deformability to  $\Lambda_{1.37M_\odot} > 210$  [12], 300 [11], 279 [13], and 309 [14].

In Ref. [15] Lattimer and Prakash have empirically observed that for densities between  $1.5n_0$  and  $2 - 3n_0$ , the radius of the star scales with  $p^{1/4}$  with  $p$  the pressure at these densities. This means that knowing the radius of a NS with sufficient precision will constrain the EoS of stellar matter in this specific range of densities. It also raises the question whether other correlations between the thermodynamic properties of nuclear matter in  $\beta$ -equilibrium and NS properties such as the radius or tidal deformability could exist. In this case further constraints on the NS EoS could be obtained thanks to new measurements of the NS tidal deformability with future LIGO/Virgo detection of gravitational waves emitted from binary NS mergers. The precise determination of the radius of NSs, in addition to their mass, expected from the currently-operating NICER

---

\* marcio.ferreira@uc.pt

mission [16], and future X-ray observatories like the Athena X-ray telescope [17] and eXTP [18] would also allow to constrain the EoS in various ranges of density.

NS properties such as the radius and mass can be obtained by solving the Tolman-Oppenheimer-Volkoff (TOV) equations [19, 20] for a static and spherical star in hydrostatic equilibrium, which requires the EoS as a input. As a consequence a one-to-one correspondence is established between the NS mass and radius and the EoS of  $\beta$ -equilibrated stellar matter. The possibility of inverting this mapping, allowing the determination of the EoS from the measurement of the mass and radius of a large number of stars was discussed by Lindblom [21]. Later, it was proposed that a smaller number of astrophysical observations is required if realistic EoS are parametrized using piecewise polytropes with transition densities from one polytrope to another chosen at well selected densities [22]. A different approach was discussed in [23], where it was shown that the determination of the pressure at three fiducial densities could be obtained from the measurement of three different NSs.

Correlations between nuclear matter parameters and NS properties have been explored using several nuclear models [24–32]. These studies, however, show a considerable model dependence since different models with similar values of the nuclear matter parameters may result in different EoSs. In the present work, we study the correlation of various astrophysical observables directly with the thermodynamical variables of the EoS to avoid the model dependence [33]. The main objective of the present work is to look for further correlations that could allow to establish constraints on the EoS of nuclear matter from the observation of NS. We use a large set of so-called meta-models that satisfy a given number of well defined nuclear matter and NS properties [34, 35].

The paper is organized as follows. In Sec. II, we introduce the EoS parametrization and generating process for the meta-models. The correlation analysis on the generated set of EoS is developed in Sec. III. Finally, the conclusions are drawn in Sec IV.

## II. EOS PARAMETRIZATION

We start from the generic functional form for the energy per particle of homogeneous nuclear matter

$$\mathcal{E}(n, \delta) = e_0(n) + e_{sym}(n)\delta^2 \quad (1)$$

where  $n = n_n + n_p$  is the baryonic density and  $\delta = (n_n - n_p)/n$  is the asymmetry with  $n_n$  and  $n_p$  being the neutron and proton densities, respectively. This approach has been applied recently in several works, [34, 36, 37]. We consider a Taylor expansion of this energy functional around the saturation density  $n_{sat}$  until

fourth order as in [34, 36]:

$$e_0(n) = E_{sat} + \frac{1}{2}K_{sat}x^2 + \frac{1}{6}Q_{sat}x^3 + \frac{1}{24}Z_{sat}x^4 \quad (2)$$

$$e_{sym}(n) = E_{sym} + L_{sym}x + \frac{1}{2}K_{sym}x^2 + \frac{1}{6}Q_{sym}x^3 + \frac{1}{24}Z_{sym}x^4 \quad (3)$$

where  $x$  is defined as  $x = (n - n_{sat})/(3n_{sat})$ . The empirical parameters can be identified as the coefficients of the expansion. The isoscalar empirical parameters are defined as proportional to successive density derivatives of  $e_0(n)$ ,

$$P_{IS}^{(k)} = (3n_{sat})^k \left. \frac{\partial^k e_0(n)}{\partial n^k} \right|_{\{\delta=0, n=n_{sat}\}}, \quad (4)$$

whereas the isovector parameters measure density derivatives of  $e_{sym}(n)$ ,

$$P_{IV}^{(k)} = (3n_{sat})^k \left. \frac{\partial^k e_{sym}(n)}{\partial n^k} \right|_{\{\delta=0, n=n_{sat}\}}. \quad (5)$$

The corresponding empirical parameters are then

$$\{E_{sat}, K_{sat}, Q_{sat}, Z_{sat}\} \rightarrow \{P_{IS}^{(0)}, P_{IS}^{(2)}, P_{IS}^{(3)}, P_{IS}^{(4)}\} \quad (6)$$

and

$$\begin{aligned} & \{E_{sym}, L_{sym}, K_{sym}, Q_{sym}, Z_{sym}\} \\ & \rightarrow \{P_{IV}^{(0)}, P_{IV}^{(1)}, P_{IV}^{(2)}, P_{IV}^{(3)}, P_{IV}^{(4)}\}. \end{aligned}$$

The coefficients of low orders are already quite well constrained experimentally [38–43], however  $Q_{sat}$ ,  $Z_{sat}$  and  $K_{sym}$ ,  $Q_{sym}$ ,  $Z_{sym}$  are only poorly known [30, 32, 36, 44–47]. The saturation energy  $E_{sat}$  and saturation density  $n_{sat}$  being rather well constrained, we fix their values throughout this work:  $E_{sat} = -15.8$  MeV (the current estimated value is  $-15.8 \pm 0.3$  MeV [34]), and  $n_{sat} = 0.155$  fm $^{-3}$ .

With this approach, each meta-model is represented by a point in the 8-dimensional space of parameters. Instead of analyzing the models on a fixed grid, we will employ random sampling of models through a multivariate Gaussian with zero covariance:

$$EoS_i = \{E_{sym}, L_{sym}, K_{sat}, K_{sym}, Q_{sat}, Q_{sym}, Z_{sat}, Z_{sym}\}_i \sim N(\boldsymbol{\mu}, \boldsymbol{\Sigma})$$

where the mean value vector and covariance matrix are, respectively,

$$\boldsymbol{\mu}^T = (\bar{E}_{sym}, \bar{L}_{sym}, \bar{K}_{sat}, \bar{K}_{sym}, \bar{Q}_{sat}, \bar{Q}_{sym}, \bar{Z}_{sat}, \bar{Z}_{sym})$$

and

$$\boldsymbol{\Sigma} = \text{diag}(\sigma_{E_{sym}}, \dots, \sigma_{Z_{sym}}).$$

In the present approach, as discussed in [34], no a-priori correlations exist between the different parameters of the EoS. However, as we will see, imposing experimental and observational constraints will give rise to correlations. The physical correlations among the empirical parameters arise from a set of physical constraints [34, 36]. The parameters of the Gaussian distributions for each parameter are in Table I.

$P_i$	Initial dist.		Final dist.	
	$\bar{P}_i$	$\sqrt{\sigma_{P_i}}$	$\bar{P}_i$	$\sqrt{\sigma_{P_i}}$
$K_{sat}$	230	20	233.35	18.24
$Q_{sat}$	300	400	56.04	122.31
$Z_{sat}$	-500	1000	-178.46	141.26
$E_{sym}$	32	2	33.33	1.89
$L_{sym}$	60	15	51.45	11.83
$K_{sym}$	-100	100	-44.24	63.24
$Q_{sym}$	0	400	237.52	299.42
$Z_{sym}$	-500	1000	372.98	698.72

Table I. The mean  $\bar{P}_i$  and standard deviation  $\sqrt{\sigma_{P_i}}$  of the multivariate Gaussian, where  $\sigma_{P_i}$  is the variance of the parameter  $P_i$ . Our EoSs are sampled using the initial distribution for  $P_i$  assuming that there are no correlations among the parameters. The final distribution for  $P_i$  are obtained after imposing the filters as listed in the text. All the quantities are in units of MeV. The values of  $E_{sat}$  and  $n_{sat}$  are fixed to  $-15.8$  MeV and  $0.155$  fm $^{-3}$ , respectively.

We impose the following conditions to get a valid EoS: i) be monotonically increasing (thermodynamic stability); ii) the speed of sound must not exceed the speed of light (causality); iii) supports a maximum mass at least as high as  $1.97M_\odot$  [1–4] (observational constraint); iv) predicts a tidal deformability of  $70 < \Lambda_{1.4M_\odot} < 580$  [7] (observational constraint); and v) the symmetry energy  $e_{sym}(n)$  is positive. All the EoS are in  $\beta$ -equilibrium. We use the SLy4 EoS for the low density region [48]. A valid EoS must cross the SLy4 EoS in the  $P(\mu)$  plane below  $n < 0.10$  fm $^{-3}$  consistently with the range of core-crust transition densities for a large set of nuclear models [27]. The SLy4 EoS is matched with the generated EoSs by requiring  $P_{SLy4}(\mu) = P_{EoS}(\mu)$  with  $\mu$  the chemical potential.

### III. RESULTS

In the present section we first discuss the properties of the set of EoS we have built after imposing the constraints listed above. Using these EoSs, we then study correlations between NS observables and the EoS properties at given densities.

#### A. Empirical parameters values and NS properties

After applying all the filters indicated above to  $10^7$  sampled EoS, we obtain 2121 valid EoS. This number is quite small and it is mainly due to the constraint of causality and the requirement that the generated EoS and the crust SLy4 EoS intersect in the  $P - \mu$  plane. Using a simple interpolation between the crust and the core at some specific density is much less restrictive and the number of valid EoS would be much larger. However, we consider it is important to carry the information contained on the Taylor expansion not only to supra-saturation densities but also to sub-saturation densities.

In Table I, the mean values and standard deviations of the EoS parameters for the final distribution, after the constraints on the EoS were imposed, are compared with the respective initial input. It is interesting to notice that well constrained parameters like  $K_{sat}$  and  $E_{sym}$ , and even  $L_{sym}$ , do not change much from the initial distribution, while the parameters connected to the high orders, such as  $Q_{sym}$  and  $Z_{sym}$ , converge to quite different mean values.

With this set of EoS, we obtain the relation between the radius  $R$  and the mass  $M$  of the NS, solving the TOV equations [19, 20], and calculate the dimensionless tidal deformability  $\Lambda$

$$\Lambda = \frac{2}{3}k_2 \left( \frac{R}{M} \right)^5, \quad (7)$$

where  $k_2$  its quadrupole tidal Love number, following Ref. [49].

In Fig. 1, we plot the  $M - R$  and the  $\Lambda - M$  relations for the set of EoS. In what follows, these results will be used to study the correlations between NS observables and thermodynamic quantities. As an example, we present in Table II the mean value and standard deviation for the tidal deformability  $\Lambda_{M_i}$  and radius  $R_{M_i}$  of stars with masses  $M_i = 1.0, 1.2, 1.4, 1.6, 1.8 M_\odot$ . The results obtained for  $M_{1.4}$  are well inside the limits imposed by GW170817 [7] for the tidal deformability  $70 < \Lambda_{1.4M_\odot} < 580$  (but notice that this is also true without imposing maximum star mass of  $1.97M_\odot$ ) and  $R = 11.9 \pm 1.4$  km. On the other hand, if the constraints set by the electromagnetic counterpart are also considered then our EoSs satisfies the lower limit determined in [12],  $\Lambda_{1.37M_\odot} > 210$ , but not the limit calculated in [11, 13, 14]: 300, 279 and 309 respectively. However, in average and within a 95% confidence interval these lower constraints are all satisfied. The set of EoSs also satisfies the condition obtained for  $R_{1.6M_\odot}$  from an existing universal relation between the critical merger remnant mass to a prompt collapse and the compactness of the maximum mass star, i.e.,  $R_{1.6M_\odot} \gtrsim 10.7$  km [50, 51].

The obtained results are also in agreement with

[52], where the maximum value  $R_{1.4M_\odot} = 13.6$  km and the minimum value  $\Lambda_{1.4M_\odot} = 120$  were reported, using a generic family of EoS that interpolate between chiral effective field theory results at low densities and perturbative QCD at high densities. Furthermore, our results are compatible with [53] (an extra condition on the allowed maximum NS mass was imposed,  $M_{\max} < 2.16M_\odot$ , though), in which a mean value of  $R_{1.4M_\odot} = 12.39$  km and a  $2\sigma$  confidence of  $12.00 < R_{1.4M_\odot}/\text{km} < 13.45$  were determined using a piecewise polytrope parametrization of the EoS, which took into account nuclear matter calculations of the outer crust, near saturation densities, and perturbative QCD.

	mean	std	min	max
$\Lambda_{1.0M_\odot}$	2967.88	283.78	1677.51	3597.70
$\Lambda_{1.2M_\odot}$	1129.15	118.90	620.60	1377.93
$\Lambda_{1.4M_\odot}$	467.53	57.89	243.53	579.93
$\Lambda_{1.6M_\odot}$	201.96	31.36	93.31	267.29
$\Lambda_{1.8M_\odot}$	87.54	18.48	29.41	126.26
$R_{1.0M_\odot}$	11.96	0.19	10.99	12.34
$R_{1.2M_\odot}$	12.09	0.19	11.07	12.48
$R_{1.4M_\odot}$	12.18	0.21	11.13	12.59
$R_{1.6M_\odot}$	12.20	0.25	11.09	12.68
$R_{1.8M_\odot}$	12.14	0.31	10.85	12.73

Table II. Sample statistics for  $\Lambda_{M_i}$  and  $R_{M_i}$  (km): mean, standard deviation, maximum, and minimum values.

Interestingly, the minimum value obtained for  $\Lambda_{1.4M_\odot}$  is 243.53 and, furthermore, only a very small percentage of the EoS failed to reproduce  $\Lambda_{1.4M_\odot} < 580$  (the maximum value reached for  $\Lambda_{1.4M_\odot}$  was 651.85). In other words, the present set of EoS describes NSs with a narrow region of  $\Lambda_{1.4M_\odot}$  with a mean value of 467.53, and fulfill  $70 < \Lambda_{1.4M_\odot} < 580$  [7].

## B. Correlation between thermodynamic quantities and NS observables

In the present section, we study the possible existing correlations between the thermodynamic properties of dense stellar matter in  $\beta$ -equilibrium and NS observables. In the following analysis we use the Pearson correlation coefficient

$$\text{Corr}[X, Y] = \frac{\langle (X - \mu_X)(Y - \mu_Y) \rangle}{\sigma_X \sigma_Y},$$

where  $\langle \dots \rangle$  is the expectation value and  $\sigma_X$  and  $\sigma_Y$  are the standard deviations of variables  $X$  and  $Y$ , respectively. In particular, we consider the correlation between the pressure in Fig. 2, the energy density in Fig. 3, and the

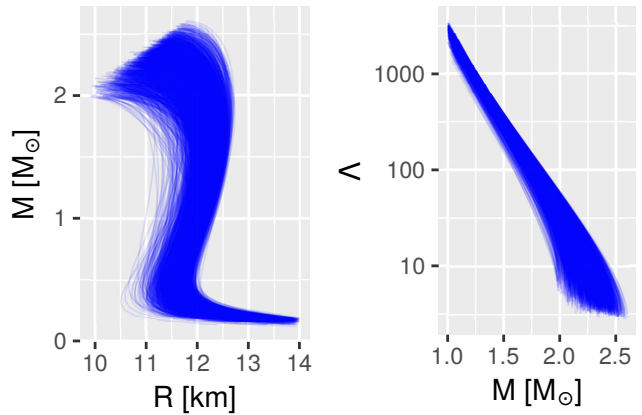


Figure 1. Mass vs. radius (left) and the mass vs. tidal deformability (right) diagrams for set of EoS built in the present study.

speed of sound in Fig. 4, at each baryonic density with the radius, tidal deformability, and Love number of NSs with  $M = 1.0, 1.2, 1.4, 1.6$  and  $1.8 M_\odot$ .

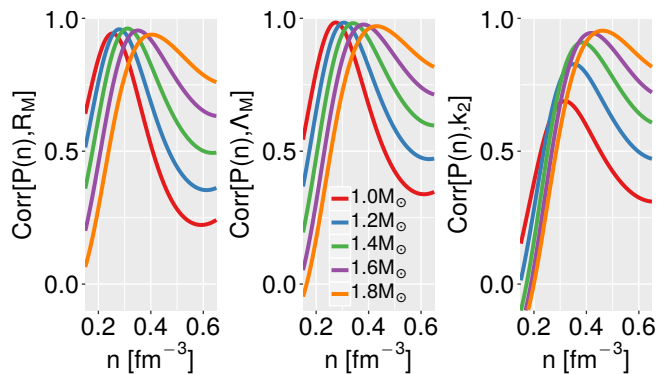


Figure 2. The density dependence of correlation coefficient of the pressure,  $P(n)$  with radius  $R$  (left), tidal deformability  $\Lambda$  (middle), and Love number  $k_2$  (right) for different NS masses as indicated obtained for Meta models.

We first discuss the correlation of the NS properties with the pressure as shown in Fig. 2. Interestingly one can identify strong correlations between the pressure and the various NS properties that we considered, at certain densities. The left panel, for example, shows how the correlation between  $P(n)$  and  $R_M$  remains quite high in a relatively small range of densities for all the five masses considered. The maximum of the correlation shifts to larger densities, from  $n \approx 0.25$  to  $0.35 \text{ fm}^{-3}$ , as the mass of the star increases. This is precisely the empirical correlation identified by Lattimer and Prakash in [15]. A similar and an even stronger correlation, with a coefficient very close to 1, is observed between the pressure and the tidal deformability in the same range of densities (center panel). The Love number  $k_2$  shows a quite strong correlation at  $n \approx 0.45 \text{ fm}^{-3}$  but only for

the larger masses (right panel).

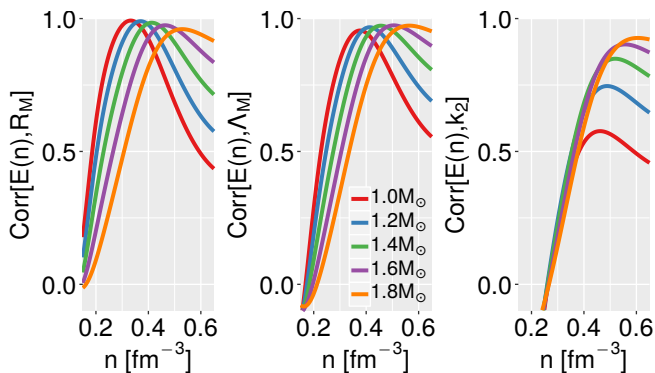


Figure 3. The density dependence of correlation coefficient of the energy density,  $E(n)$ , with radius  $R$  (left), tidal deformability  $\Lambda$  (middle), and Love number  $k_2$  (right) for different NS masses as indicated obtained for Meta models.

The correlations between NS observables and the energy density are shown in Fig. 3. Again, strong correlations are identified with all the NS observables but at larger densities,  $n \approx 0.32$  to  $0.5 \text{ fm}^{-3}$  with the smaller (larger) masses closer to the smaller (larger) value. Similar to the case of pressure, the correlation between the energy density and  $\Lambda$  remains strong for all NS masses. The maximum correlation is obtained at higher densities when massive NS are considered.

Finally, for the speed of sound shown in Fig. 4 strong correlations are again present but occurring at smaller densities than the ones obtained for the pressure, i.e. at densities  $\approx 0.2 - 0.3 \text{ fm}^{-3}$ .

A strong correlation, i.e.,  $\text{Corr} \approx 1$ , means that the sample variance of the NS observable is almost entirely linearly explained by the variance of the thermodynamical quantity. Therefore, one can use the NS observable as a way to constrain the thermodynamical quantities at different baryon densities.

It is interesting to compare our results, obtained from a Taylor expansion parametrized around saturation density, with nuclear models EoS. We use a dataset of unified EOS based on 24 Skyrme interactions and 26 relativistic mean-field nuclear parametrizations (some of them including a transition to hyperonic matter at high density) [54]. The constraints  $70 < \Lambda_{1.4M_\odot} < 580$  and  $M_{\text{max}} > 1.97M_\odot$  are fulfilled by the following models: BSk20, BSk21 [55], BSk25, BSk26 [56], SKa, SKb [57], SkI4 [58], SkI6 [59], SkMP [60], SKOp [61], SLy2, SLy9 [62], SLy230a [63], SLy4 [64]. In Fig. 5 we show the variation with the density of the correlation coefficient between  $P$ ,  $E$ , and  $v_s$  and the NS properties  $R$ ,  $\Lambda$  and  $k_2$  for different masses. When we compare the pressure correlations in Fig. 2 and in top panel of Fig. 5, we notice that the main difference occurs at high densities  $n > 0.6 \text{ fm}^{-3}$ , where the nuclear models show a

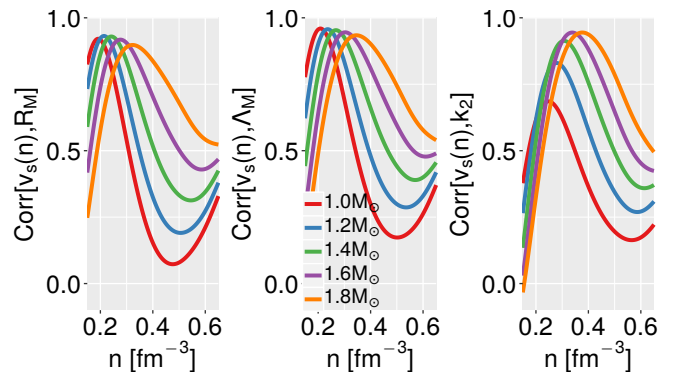


Figure 4. The density dependence of correlation coefficient of the sound velocity,  $v_s(n)$ , with radius  $R$  (left), tidal deformability  $\Lambda$  (middle), and Love number  $k_2$  (right) for different NS masses as indicated obtained for Meta models.

stronger correlation with all NS observables. We indicate in Table III the maximum correlation obtained for  $M = 1.4M_\odot$  and the densities at which they occur for the nuclear models. For reference, the correlation coefficient at the same densities obtained for our EoSs from constrained meta-models are also given. We see that the maximum correlations happen at nearly the same densities. The correlations of NS properties with the energy density obtained for our set of EoSs from meta-models (Fig 3) and those for nuclear models (middle panel of Fig. 5) show overall similar trends. The fact that for our EoSs, the correlations are more suppressed at high densities may be due to the differences in the high density behavior.

Models			Nuclear	Meta
		$n$	corr	corr
$P(n)$	$\Lambda_{1.4M_\odot}$	0.320	0.992	0.891
$P(n)$	$R_{1.4M_\odot}$	0.281	0.980	0.937
$e(n)$	$\Lambda_{1.4M_\odot}$	0.544	0.978	0.914
$e(n)$	$R_{1.4M_\odot}$	0.442	0.995	0.974
$v_s(n)$	$\Lambda_{1.4M_\odot}$	0.219	0.987	0.870
$v_s(n)$	$R_{1.4M_\odot}$	0.195	0.964	0.844

Table III. Densities of maximum correlations for the nuclear models and the correlation value at those densities for our set obtained from meta-models (last column).

### C. Constraining the thermodynamical properties

In the previous section, we saw that all thermodynamical quantities show strong correlations with NS observables, specially the radius and the tidal deformability, in some specific range of density. We now study how to use these linear dependences to constrain the thermodynamical quantities from future measurements

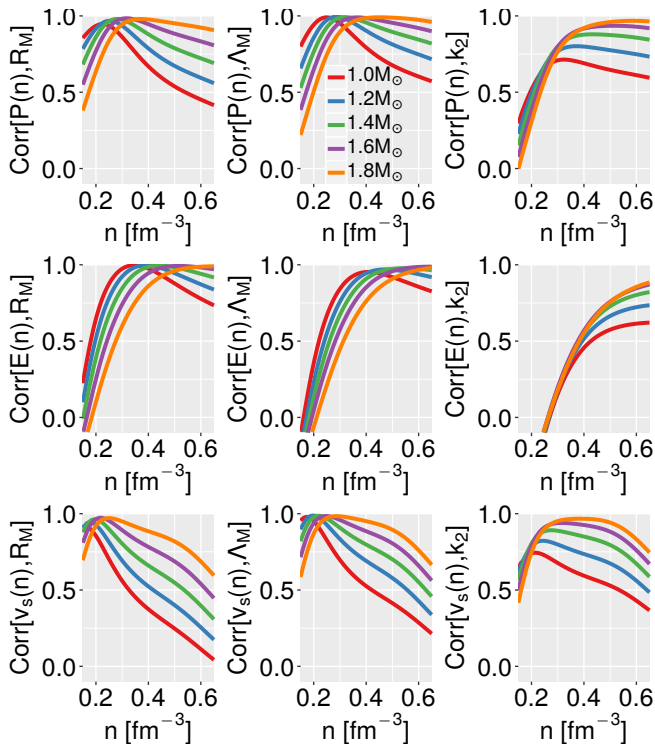


Figure 5. The density dependence of correlation coefficient of the pressure  $P(n)$  (top row), energy density  $E(n)$  (middle row), and sound velocity  $v_s(n)$  (bottom row) with radius  $R$  (left), tidal deformability  $\Lambda$  (middle), and Love number  $k_2$  (right) for different NS masses as indicated obtained for a diverse set of nuclear models.

of the radius and the tidal deformability for a canonical NS,  $M = 1.4M_\odot$ .

Fig. 6 shows the density at which the correlation is maximum between both the tidal deformability (top panels) and radius (bottom panels) with the energy density (left), pressure (middle), and sound velocity (right) of a  $1.4M_\odot$  star. The regression analysis is summarized in Table IV for three NS masses:  $1.0M_\odot$ ,  $1.4M_\odot$  (shown in Fig. 6), and  $1.8M_\odot$ . Recently, the first simultaneous determination of the radius and mass of a NS with the NICER mission was obtained after the modeling the pulsating X-ray emission from the isolated millisecond pulsar PSR J0030+0451:  $R \sim 11.5 - 14$  km for  $M \sim 1.4M_\odot$  [65–67]. If a more precise radius measurement becomes available, one would then be able to immediately get constraints on the EoS at three different densities: the energy density at  $0.413 \text{ fm}^{-3}$ , the pressure at  $0.311 \text{ fm}^{-3}$  and the sound velocity at  $0.250 \text{ fm}^{-3}$ . Similar constraints could also be derived from the observation of another NS, one of the primary targets PSR J0437–4715 with a mass  $1.44 \pm 0.07M_\odot$  [16, 68]. If besides also information on the radius of the massive pulsar PSR J1614–2230 ( $M = 1.908 \pm 0.018M_\odot$ ) would be measured we would be able to get further constraints on the EoS for other dif-

ferent densities.

From Table IV, using the maximum and the minimum  $\Lambda_{1.4M_\odot}$  calculated from our EoS set (see Table II), we constrain the thermodynamical quantities at different densities

$$P(n = 0.340 \text{ fm}^{-3}) = [17.82, 34.56] \text{ MeV/fm}^3 \quad (8)$$

$$E(n = 0.456 \text{ fm}^{-3}) = [452.22, 468.22] \text{ MeV/fm}^3 \quad (9)$$

$$v_s(n = 0.266 \text{ fm}^{-3}) = [0.325, 0.446] \text{ units of } c. \quad (10)$$

Doing the same analysis for  $R_{1.4M_\odot}$ , using our sample max/min values, we get

$$P(n = 0.311 \text{ fm}^{-3}) = [11.66, 25.27] \text{ MeV/fm}^3 \quad (11)$$

$$E(n = 0.413 \text{ fm}^{-3}) = [403.98, 416.78] \text{ MeV/fm}^3 \quad (12)$$

$$v_s(n = 0.242 \text{ fm}^{-3}) = [0.278, 0.395] \text{ units of } c. \quad (13)$$

These results are summarized in Table V. We also include, in the same Table, the constraints on  $P$ ,  $E$ , and  $v_s$  obtained from the LIGO/Virgo GW170817 analysis [7]. Confidence intervals (on the marginalized posterior) for the pressure were determined in [7]. The 90% credible level is  $P(n = 0.311 \text{ fm}^{-3}) = [8.79, 31.09] \text{ MeV/fm}^3$  and  $P(n = 0.340 \text{ fm}^{-3}) = [12.01, 41.39] \text{ MeV/fm}^3$ , while the 50% credible level is  $P(n = 0.311 \text{ fm}^{-3}) = [11.95, 23.66] \text{ MeV/fm}^3$  and  $P(n = 0.340 \text{ fm}^{-3}) = [16.37, 32.00] \text{ MeV/fm}^3$ . Our results, Eqs. (8) and (11), are in good agreement even at the 50% credible level. We should note, however, that the EoSs used in [7] have lower  $\Lambda_{1.4M_\odot}$  values, which are not represented in our dataset. Assuming that the correlations that we have obtained are model-independent, as the analysis of the nuclear models seems to suggest, one may use the regression analysis in Table IV to constrain the pressure at any given value of  $\Lambda_{1.4M_\odot}$  (the same applies to  $R_{1.4M_\odot}$ ). We get for  $70 < \Lambda_{1.4M_\odot} < 580$ ,  $P(0.340 \text{ fm}^{-3}) = [9.19, 34.56] \text{ MeV/fm}^3$ , which is close to the interval determined in [7]. Furthermore, additional constraints on the energy density and sound velocity can be determined from  $70 < \Lambda_{1.4M_\odot} < 580$ . They are listed in Table V.

In Fig. 7 we show the constraints on the pressure at different densities which one can obtain from measurements of the radius and tidal deformability for NSs of various masses. For the radius, we adopt the masses of  $M = 1.3, 1.4$  and  $1.5M_\odot$ , which covers the range of values for most observed NSs in particular the NICER targets PSR J0030+0451 and PSR J0437–4715 and  $M = 1.8$  and  $1.9M_\odot$  to explore the consequence of the radius determination of a massive NS such as PSR J1614–2230. For the tidal deformability we restrict ourselves to  $M = 1.3$  and  $1.4M_\odot$  as this corresponds to the mass range of NSs currently observed in a binary with another NS [69]. The vertical error bars (hardly visible) for constraints from the tidal deformabilities account for the errors in the determination of the slope and the interception in the linear regression with the pressure (parameters  $m$  and  $b$  in Table IV). For medium-range masses  $M \sim 1.4M_\odot$  the future determination of the tidal deformability will allow

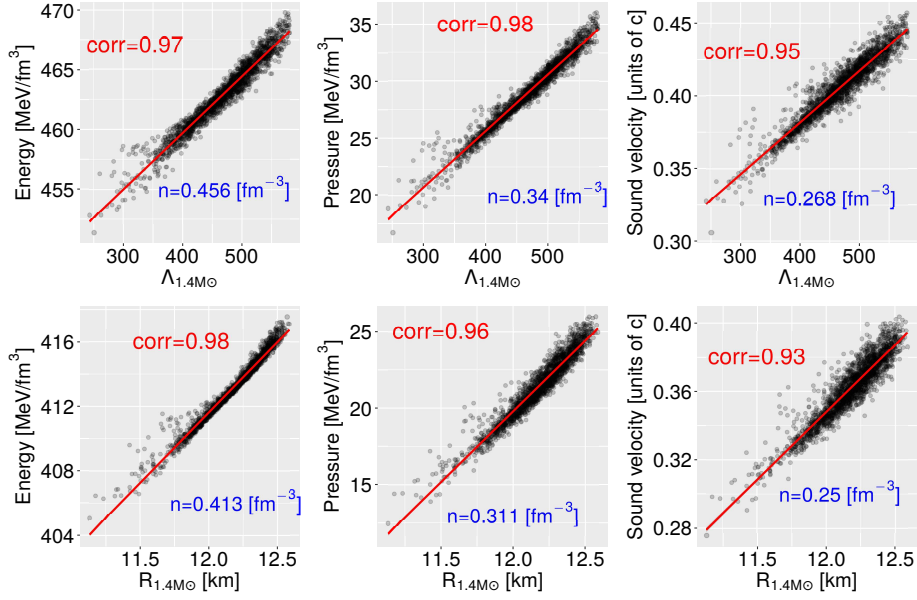


Figure 6.  $\Lambda_{1.4M_\odot}$  (top) and  $R_{1.4M_\odot}$  (bottom) as a function of the energy density (left), the pressure (middle) and the speed of sound (right) for all meta models at the densities corresponding to the maximum correlations. These densities and correlation coefficient are indicated in each of the panels.

$n$	$Q$	$Z$	Corr[ $Q, Z$ ]	$m$	$b$
0.275	$P(n)$	$\Lambda_{1.0M_\odot}$	0.984	$(4.453 \pm 0.017) \times 10^{-3}$	$0.827 \pm 0.052$
0.340		$\Lambda_{1.4M_\odot}$	0.982	$(49.389 \pm 0.209) \times 10^{-3}$	$5.898 \pm 0.098$
0.430		$\Lambda_{1.8M_\odot}$	0.970	$(43.10 \pm 0.23) \times 10^{-2}$	$24.78 \pm 0.21$
0.254	$E(n)$	$R_{1.0M_\odot}$	0.943	$(503.89 \pm 3.86) \times 10^{-2}$	$-49.04 \pm 0.46$
0.311		$R_{1.4M_\odot}$	0.962	$(942.68 \pm 5.85) \times 10^{-2}$	$-91.11 \pm 0.70$
0.403		$R_{1.8M_\odot}$	0.939	$(1885.9 \pm 15.0) \times 10^{-2}$	$-171.6 \pm 1.8$
0.377	$v_s(n)$	$\Lambda_{1.0M_\odot}$	0.955	$(4.4 \pm 0.0) \times 10^{-3}$	$359.8 \pm 0.1$
0.456		$\Lambda_{1.4M_\odot}$	0.973	$(47.4 \pm 0.2) \times 10^{-3}$	$440.9 \pm 0.1$
0.564		$\Lambda_{1.8M_\odot}$	0.973	$(374.7 \pm 1.9) \times 10^{-3}$	$564.8 \pm 0.2$
0.333	$v_s(n)$	$R_{1.0M_\odot}$	0.992	$(4583.9 \pm 12.3) \times 10^{-3}$	$271.3 \pm 0.1$
0.413		$R_{1.4M_\odot}$	0.984	$(8823.4 \pm 34.4) \times 10^{-3}$	$306.8 \pm 0.4$
0.529		$R_{1.8M_\odot}$	0.960	$(1628.0 \pm 10.3) \times 10^{-2}$	$354.5 \pm 1.3$
0.209	$v_s(n)$	$\Lambda_{1.0M_\odot}$	0.960	$(4.908 \pm 0.031) \times 10^{-5}$	$0.160 \pm 0.001$
0.268		$\Lambda_{1.4M_\odot}$	0.953	$(0.361 \pm 0.002) \times 10^{-3}$	$0.239 \pm 0.001$
0.346		$\Lambda_{1.8M_\odot}$	0.934	$(1.918 \pm 0.016) \times 10^{-3}$	$0.360 \pm 0.001$
0.192	$v_s(n)$	$R_{1.0M_\odot}$	0.921	$(66.371 \pm 0.610) \times 10^{-3}$	$-0.507 \pm 0.007$
0.242		$R_{1.4M_\odot}$	0.930	$(80.609 \pm 0.694) \times 10^{-3}$	$-0.604 \pm 0.008$
0.323		$R_{1.8M_\odot}$	0.898	$(93.086 \pm 0.992) \times 10^{-3}$	$-0.620 \pm 0.012$

Table IV. Maximum correlations,  $\text{Corr}[Q, Z]$ , between the thermodynamic properties,  $Q = \{P(n), E(n), v_s(n)\}$ , and the NS properties,  $Z = \{\Lambda_{M_i}, R_{M_i}\}$ . We show the linear regression analysis for  $Q = m \times Z + b$  at a fixed density  $n$ . In the table  $b$  has the units of  $Q$  ( $\text{MeV}/\text{fm}^3$  for  $P$  and  $E$  and  $c$  for  $v_s$ ) and  $m$  has the units of  $Z/Q$ , i.e.  $Q^{-1}$  for  $Z = \Lambda$  and  $\text{km}/Q^{-1}$  for  $Z = R$ .

to constrain the pressure at densities  $\sim 10\%$  larger than that for the radius. In addition, measuring the radius of

a massive NS would allow us to put limits at the pressure for larger densities. Thus observational constraints

Bounds		$P(0.340)$		$E(0.456)$		$v_s(0.268)$	
		[MeV fm <sup>-3</sup> ]		[MeV fm <sup>-3</sup> ]		[c]	
		min	max	min	max	min	max
$\Lambda_{1.4M_\odot}$	243.53 – 579.93	17.82	34.56	452.22	468.22	0.325	0.446
	70 – 580 [7]	9.19	34.56	443.96	468.23	0.262	0.446
Bounds		$P(0.311)$		$E(0.413)$		$v_s(0.242)$	
		[MeV fm <sup>-3</sup> ]		[MeV fm <sup>-3</sup> ]		[c]	
		min	max	min	max	min	max
$R_{1.4M_\odot}$	11.13 – 12.59	11.66	25.27	403.98	416.78	0.278	0.395
	10.5 – 13.3 [7]	5.74	31.93	398.40	423.05	0.227	0.453

Table V. Constraints on pressure  $P(n)$ , energy density  $E(n)$  and sound velocity  $v_s(n)$  for  $\beta$ -equilibrium matter at density  $n(\text{fm}^{-3})$  obtained from bounds on tidal deformability and radius for neutron star with canonical mass  $1.4M_\odot$  using our EoSs. Constraints obtained from the LIGO/Virgo analysis are also shown (see text).

on NS properties from multi-messenger astrophysics will enable us to infer the properties of NS matter in the range  $1 - 3n_0$  which we can not probe in terrestrial laboratories.

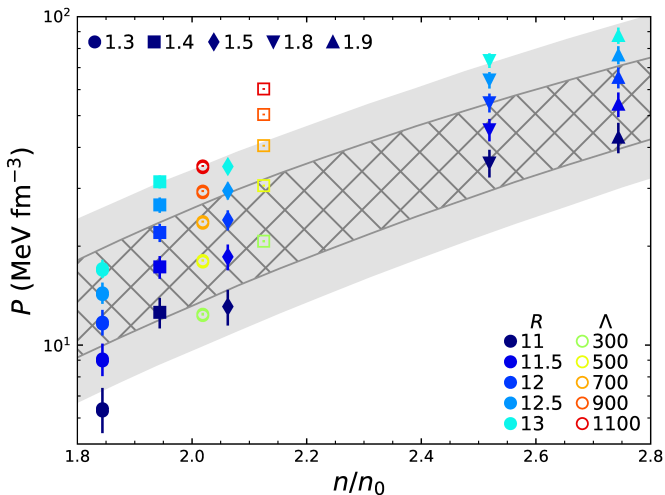


Figure 7. Constraints on the pressure obtained at different densities (expressed in units of the nuclear saturation density) from measurements of the radius (full symbols) and tidal deformabilities (empty symbols) of NSs of different masses (shown by different types of symbols). The outer (inner) gray region is the 90% credible level (50% credible level) from [7]. See text for details.

#### IV. CONCLUSIONS

We found strong correlations between the thermodynamical properties, i.e., the pressure, energy density and sound velocity with the radius and the tidal deformability of NS over a wide range of masses. These correlations were obtained from a set of EoS parametrized by a Taylor expansion around the saturation density. Similar correlations are confirmed using EoS obtained from nuclear

models, indicating that they are model-independent. It is shown that for a given NS mass, there is always a density where the tidal deformability and the radius are highly correlated with the pressure, energy density, and speed of sound. A single determination of the tidal deformability ( $\Lambda_{M_i}$ ) or radius ( $R_{M_i}$ ) of a NS of mass  $M_i$  allows to constrain the thermodynamic properties at three distinct but close densities. For a  $1.4M_\odot$  NS, the pressure could be constrained at  $n \approx 2n_0$ , the energy density at  $n \approx 2.7n_0$ , and the sound velocity at  $n \approx 1.7n_0$ .

We show that the radius and tidal deformability of NSs for different masses are strongly correlated with thermodynamic variables of EoS at supra-saturation densities in the range of  $n \approx 1 - 3n_0$ . The precise measurement of the radius of the pulsars PSR J0030+0451 and PSR J0437–4715 with a mass  $\sim 1.4M_\odot$  by the NICER mission would allow us to get immediately information on the EoS at three different densities, the pressure at  $\sim 2n_0$ , the energy density at  $\sim 2.5n_0$ , and the sound velocity at  $\sim 1.5n_0$ . Complementing this information with the further radius measurement, for example, of PSR J1614-2230 with  $M \simeq 1.9M_\odot$  and constraints on the tidal deformability of various NSs from the observations of GW from merging binary NS systems would set very stringent constraints on the EoS at supra-saturation densities. It may be pointed out that if a phase transition to a quark phase takes place, this will occur at densities close to or beyond  $3n_0$ , therefore it will may not significantly affect the correlations obtained in the present work, as they are connected to the hadronic phase.

#### ACKNOWLEDGMENTS

This article is based upon work partially funded by COST Action CA16214 PHAROS supported by COST (European Cooperation in Science and Technology), and by the FCT (Portugal) Projects No.UID/FIS/04564/2019 and POCI-01-0145-FEDER-



029912 and the Polish National Science Centre (NCN) under the grant No. 2017/26/D/ST9/00591. T.M acknowledge the Council of Scientific and Industrial Re-

search (CSIR), Human Resource Development, Govt. of India for the support of International Travel Grant TG/10542/19-HRD.

- 
- [1] Z. Arzoumanian et al. (NANOGrav), *Astrophys. J. Suppl.* **235**, 37 (2018), arXiv:1801.01837 [astro-ph.HE].
- [2] E. Fonseca et al., *Astrophys. J.* **832**, 167 (2016), arXiv:1603.00545 [astro-ph.HE].
- [3] P. Demorest, T. Pennucci, S. Ransom, M. Roberts, and J. Hessels, *Nature* **467**, 1081 (2010).
- [4] J. Antoniadis, P. C. C. Freire, N. Wex, T. M. Tauris, R. S. Lynch, M. H. van Kerkwijk, M. Kramer, C. Bassa, V. S. Dhillon, T. Driebe, J. W. T. Hessels, V. M. Kaspi, V. I. Kondratiev, N. Langer, T. R. Marsh, M. A. McLaughlin, T. T. Pennucci, S. M. Ransom, I. H. Stairs, J. van Leeuwen, J. P. W. Verbiest, and D. G. Whelan, *Science* **340**, 448 (2013).
- [5] H. T. Cromartie et al., (2019), 10.1038/s41550-019-0880-2, arXiv:1904.06759 [astro-ph.HE].
- [6] B. P. Abbott et al. (LIGO Scientific, Virgo), *Phys. Rev. Lett.* **119**, 161101 (2017), arXiv:1710.05832 [gr-qc].
- [7] B. P. Abbott et al. (Virgo, LIGO Scientific), *Phys. Rev. Lett.* **121**, 161101 (2018), arXiv:1805.11581 [gr-qc].
- [8] B. P. Abbott et al. (LIGO Scientific, Virgo, Fermi-GBM, INTEGRAL), *Astrophys. J.* **848**, L13 (2017), arXiv:1710.05834 [astro-ph.HE].
- [9] B. P. Abbott et al. (LIGO Scientific, Virgo, Fermi GBM, INTEGRAL, IceCube, AstroSat Cadmium Zinc Telluride Imager Team, IPN, Insight-Hxmt, ANTARES, Swift, AGILE Team, 1M2H Team, Dark Energy Camera GW-EM, DES, DLT40, GRAWITA, Fermi-LAT, ATCA, ASKAP, Las Cumbres Observatory Group, OzGrav, DWF (Deeper Wider Faster Program), AST3, CAAS-TRO, VINROUGE, MASTER, J-GEM, GROWTH, JAGWAR, CaltechNRAO, TTU-NRAO, NuSTAR, Pan-STARRS, MAXI Team, TZAC Consortium, KU, Nordic Optical Telescope, ePESSTO, GROND, Texas Tech University, SALT Group, TOROS, BOOTES, MWA, CALET, IKI-GW Follow-up, H.E.S.S., LOFAR, LWA, HAWC, Pierre Auger, ALMA, Euro VLBI Team, Pi of Sky, Chandra Team at McGill University, DFN, ATLAS Telescopes, High Time Resolution Universe Survey, RIMAS, RATIR, SKA South Africa/MeerKAT), *Astrophys. J.* **848**, L12 (2017), arXiv:1710.05833 [astro-ph.HE].
- [10] D. Radice, S. Bernuzzi, W. Del Pozzo, L. F. Roberts, and C. D. Ott, *Astrophys. J.* **842**, L10 (2017), arXiv:1612.06429 [astro-ph.HE].
- [11] D. Radice, A. Perego, F. Zappa, and S. Bernuzzi, *Astrophys. J.* **852**, L29 (2018), arXiv:1711.03647 [astro-ph.HE].
- [12] A. Bauswein, N.-U. Friedrich Bastian, D. Blaschke, K. Chatziioannou, J. A. Clark, T. Fischer, H.-T. Janka, O. Just, M. Oertel, and N. Stergioulas, *AIP Conf. Proc.* **2127**, 020013 (2019), arXiv:1904.01306 [astro-ph.HE].
- [13] M. W. Coughlin et al., *Mon. Not. Roy. Astron. Soc.* **480**, 3871 (2018), arXiv:1805.09371 [astro-ph.HE].
- [14] Y.-Z. Wang, D.-S. Shao, J.-L. Jiang, S.-P. Tang, X.-X. Ren, F.-W. Zhang, Z.-P. Jin, Y.-Z. Fan, and D.-M. Wei, *Astrophys. J.* **877**, 2 (2019), arXiv:1811.02558 [astro-ph.HE].
- [15] J. M. Lattimer and M. Prakash, *Astrophys. J.* **550**, 426 (2001), arXiv:astro-ph/0002232 [astro-ph].
- [16] K. C. Gendreau, Z. Arzoumanian, and T. Okajima (2012) p. 844313.
- [17] C. Motch, J. Wilms, D. Barret, W. Becker, S. Bogdanov, L. Boirin, S. Corbel, E. Cackett, S. Campana, D. de Martino, F. Haberl, J. in't Zand, M. Méndez, R. Mignani, J. Miller, M. Orío, D. Psaltis, N. Rea, J. Rodriguez, A. Rozanska, A. Schwöpe, A. Steiner, N. Webb, L. Zampieri, and S. Zane, arXiv e-prints, arXiv:1306.2334 (2013), arXiv:1306.2334 [astro-ph.HE].
- [18] A. L. Watts, W. Yu, J. Poutanen, S. Zhang, S. Bhattacharyya, S. Bogdanov, L. Ji, A. Patruno, T. E. Riley, P. Bakala, A. Baykal, F. Bernardini, I. Bombaci, E. Brown, Y. Cavecchi, D. Chakrabarty, J. Chenevez, N. Degenaar, M. Del Santo, T. Di Salvo, V. Doroshenko, M. Falanga, R. D. Ferdman, M. Feroci, A. F. Gambino, M. Ge, S. K. Greif, S. Guillot, C. Gungor, D. H. Hartmann, K. Hebel, A. Heger, J. Homan, R. Iaria, J. i. Zand, O. Kargaltsev, A. Kurkela, X. Lai, A. Li, X. Li, Z. Li, M. Linares, F. Lu, S. Mahmoodifar, M. Méndez, M. Coleman Miller, S. Morsink, J. Nättilä, A. Possenti, C. Prescod-Weinstein, J. Qu, A. Riggio, T. Salmi, A. Sanna, A. Santangelo, H. Schatz, A. Schwenk, L. Song, E. Šrámková, B. Stappers, H. Stiele, T. Strohmayer, I. Tews, L. Tolos, G. Török, D. Tsang, M. Urbanec, A. Vacchi, R. Xu, Y. Xu, S. Zane, G. Zhang, S. Zhang, W. Zhang, S. Zheng, and X. Zhou, *Science China Physics, Mechanics, and Astronomy* **62**, 29503 (2019), arXiv:1812.04021 [astro-ph.HE].
- [19] R. C. Tolman, *Phys. Rev.* **55**, 364 (1939).
- [20] J. R. Oppenheimer and G. M. Volkoff, *Phys. Rev.* **55**, 374 (1939).
- [21] L. Lindblom, *Astrophys. J.* **398**, 569 (1992).
- [22] J. S. Read, B. D. Lackey, B. J. Owen, and J. L. Friedman, *Phys. Rev.* **D79**, 124032 (2009), arXiv:0812.2163 [astro-ph].
- [23] F. Özel and D. Psaltis, *Phys. Rev.* **D80**, 103003 (2009), arXiv:0905.1959 [astro-ph.HE].
- [24] I. Vidana, C. Providencia, A. Polls, and A. Rios, *Phys. Rev.* **C80**, 045806 (2009), arXiv:0907.1165 [nucl-th].
- [25] J. Xu, L.-W. Chen, B.-A. Li, and H.-R. Ma, *Astrophys. J.* **697**, 1549 (2009), arXiv:0901.2309 [astro-ph.SR].
- [26] C. Ducoin, J. Margueron, and C. Providencia, *EPL* **91**, 32001 (2010), arXiv:1004.5197 [nucl-th].

- [27] C. Ducoin, J. Margueron, C. Providencia, and I. Vidana, *Phys. Rev.* **C83**, 045810 (2011), arXiv:1102.1283 [nucl-th].
- [28] W. G. Newton, M. Gearheart, and B.-A. Li, *Astrophys. J. Suppl.* **204**, 9 (2013), arXiv:1110.4043 [astro-ph.SR].
- [29] N. Alam, B. K. Agrawal, M. Fortin, H. Pais, C. Providência, A. R. Raduta, and A. Sulaksono, *Phys. Rev.* **C94**, 052801 (2016), arXiv:1610.06344 [nucl-th].
- [30] T. Malik, N. Alam, M. Fortin, C. Providência, B. K. Agrawal, T. K. Jha, B. Kumar, and S. K. Patra, *Phys. Rev.* **C98**, 035804 (2018), arXiv:1805.11963 [nucl-th].
- [31] Z. Carson, A. W. Steiner, and K. Yagi, *Phys. Rev.* **D99**, 043010 (2019), arXiv:1812.08910 [gr-qc].
- [32] N.-B. Zhang, B.-A. Li, and J. Xu, *Astrophys. J.* **859**, 90 (2018), arXiv:1801.06855 [nucl-th].
- [33] C. Y. Tsang, M. B. Tsang, P. Danielewicz, W. G. Lynch, and F. J. Fattoyev, *Phys. Lett.* **B796**, 1 (2019), arXiv:1905.02601 [nucl-th].
- [34] J. Margueron, R. Hoffmann Casali, and F. Gulminelli, *Phys. Rev.* **C97**, 025805 (2018), arXiv:1708.06894 [nucl-th].
- [35] M. Ferreira and C. Providência, (2019), arXiv:1910.05554 [nucl-th].
- [36] J. Margueron, R. Hoffmann Casali, and F. Gulminelli, *Phys. Rev.* **C97**, 025806 (2018), arXiv:1708.06895 [nucl-th].
- [37] J. Margueron and F. Gulminelli, *Phys. Rev.* **C99**, 025806 (2019), arXiv:1807.01729 [nucl-th].
- [38] D. H. Youngblood, H. L. Clark, and Y. W. Lui, *Phys. Rev. Lett.* **82**, 691 (1999).
- [39] J. Margueron and E. Khan, *Phys. Rev.* **C86**, 065801 (2012), arXiv:1203.2134 [nucl-th].
- [40] B.-A. Li and X. Han, *Phys. Lett.* **B727**, 276 (2013), arXiv:1304.3368 [nucl-th].
- [41] J. M. Lattimer and Y. Lim, *Astrophys. J.* **771**, 51 (2013).
- [42] J. R. Stone, N. J. Stone, and S. A. Moszkowski, *Phys. Rev.* **C89**, 044316 (2014), arXiv:1404.0744 [nucl-th].
- [43] M. Oertel, M. Hempel, T. Klähn, and S. Typel, *Rev. Mod. Phys.* **89**, 015007 (2017).
- [44] M. Farine, J. M. Pearson, and F. Tondeur, *Nucl. Phys.* **A615**, 135 (1997).
- [45] J. N. De, S. K. Samaddar, and B. K. Agrawal, *Phys. Rev.* **C92**, 014304 (2015), arXiv:1506.06461 [nucl-th].
- [46] C. Mondal, B. K. Agrawal, J. N. De, and S. K. Samaddar, *Phys. Rev.* **C93**, 044328 (2016).
- [47] B.-A. Li, P. G. Krastev, D.-H. Wen, W.-J. Xie, and N.-B. Zhang, *AIP Conf. Proc.* **2127**, 020018 (2019).
- [48] F. Douchin and P. Haensel, *Astron. Astrophys.* **380**, 151 (2001), arXiv:astro-ph/0111092 [astro-ph].
- [49] T. Hinderer, *Astrophys. J.* **677**, 1216 (2008), arXiv:0711.2420 [astro-ph].
- [50] A. Bauswein, O. Just, H.-T. Janka, and N. Stergioulas, *Astrophys. J.* **850**, L34 (2017), arXiv:1710.06843 [astro-ph.HE].
- [51] S. Köppel, L. Bovard, and L. Rezzolla, *Astrophys. J.* **872**, L16 (2019), arXiv:1901.09977 [gr-qc].
- [52] E. Annala, T. Gorda, A. Kurkela, and A. Vuorinen, *Phys. Rev. Lett.* **120**, 172703 (2018).
- [53] E. R. Most, L. R. Weih, L. Rezzolla, and J. Schaffner-Bielich, *Phys. Rev. Lett.* **120**, 261103 (2018).
- [54] M. Fortin, M. Oertel, and C. Providência, *Publ. Astron. Soc. Austral.* **35**, 44 (2018), arXiv:1711.09427 [astro-ph.HE].
- [55] S. Goriely, N. Chamel, and J. M. Pearson, *Physical Review C - Nuclear Physics* **82**, 35804 (2010).
- [56] S. Goriely, N. Chamel, and J. M. Pearson, *Physical Review C - Nuclear Physics* **88**, 24308 (2013).
- [57] H. S. Kohler, *Nuclear Physics A* **258**, 301 (1976).
- [58] P. G. Reinhard and H. Flocard, *Nuclear Physics, Section A* **584**, 467 (1995).
- [59] W. Nazarewicz, J. Dobaczewski, T. R. Werner, J. A. Maruhn, P. G. Reinhard, K. Rutz, C. R. Chinn, A. S. Umar, and M. R. Strayer, *Physical Review C - Nuclear Physics* **53**, 740 (1996).
- [60] L. Bennour, P.-H. Heenen, P. Bonche, J. Dobaczewski, and H. Flocard, *Phys. Rev.* **C40**, 2834 (1989).
- [61] P. G. Reinhard, *Nucl. Phys.* **A649**, 305 (1999).
- [62] E. Chabanat, Ph.D. thesis, University Claude Bernard Lyon-1, Lyon, France (1995).
- [63] E. Chabanat, J. Meyer, P. Bonche, R. Schaeffer, and P. Haensel, *Nucl. Phys.* **A627**, 710 (1997).
- [64] E. Chabanat, P. Bonche, P. Haensel, J. Meyer, and R. Schaeffer, *Nucl. Phys.* **A635**, 231 (1998), [Erratum: *Nucl. Phys.*A643,441(1998)].
- [65] T. E. Riley, A. L. Watts, S. Bogdanov, P. S. Ray, R. M. Ludlam, S. Guillot, Z. Arzoumanian, C. L. Baker, A. V. Bilous, D. Chakrabarty, K. C. Gendreau, A. K. Harding, W. C. G. Ho, J. M. Lattimer, S. M. Morsink, and T. E. Strohmayer, arXiv e-prints , arXiv:1912.05702 (2019), arXiv:1912.05702 [astro-ph.HE].
- [66] G. Raaijmakers, T. E. Riley, A. L. Watts, S. K. Greif, S. M. Morsink, K. Hebeler, A. Schwenk, T. Hinderer, S. Nissanke, S. Guillot, Z. Arzoumanian, S. Bogdanov, D. C. K. C. Gendreau, W. C. G. Ho, J. M. Lattimer, R. M. Ludlam, and M. T. Wolff, arXiv e-prints , arXiv:1912.05703 (2019), arXiv:1912.05703 [astro-ph.HE].
- [67] M. C. Miller, F. K. Lamb, A. J. Dittmann, S. Bogdanov, Z. Arzoumanian, K. C. Gendreau, S. Guillot, A. K. Harding, W. C. G. Ho, J. M. Lattimer, R. M. Ludlam, S. Mahmoodifar, S. M. Morsink, P. S. Ray, T. E. Strohmayer, K. S. Wood, T. Enoto, R. Foster, T. Okajima, G. Prigozhin, and Y. Soong, arXiv e-prints , arXiv:1912.05705 (2019), arXiv:1912.05705 [astro-ph.HE].
- [68] A. L. Watts, N. Andersson, D. Chakrabarty, M. Feroci, K. Hebeler, G. Israel, F. K. Lamb, M. C. Miller, S. Morsink, F. Özel, A. Patruno, J. Poutanen, D. Psaltis, A. Schwenk, A. W. Steiner, L. Stella, L. Tolos, and M. van der Klis, *Reviews of Modern Physics* **88**, 021001 (2016), arXiv:1602.01081 [astro-ph.HE].
- [69] J. Alsing, H. O. Silva, and E. Berti, *Mon. Not. Roy. Astron. Soc.* **478**, 1377 (2018), arXiv:1709.07889 [astro-ph.HE].